Author Manuscript

Author Manuscript

Author Manuscript

Author Manuscript

HHS Public Access

Author manuscript

Magn Reson Med. Author manuscript; available in PMC 2019 February 01.

Published in final edited form as:

Magn Reson Med. 2018 February ; 79(2): 683–691. doi:10.1002/mrm.26715.

Super-Resolution Intracranial Quiescent Interval Slice-Selective Magnetic Resonance Angiography

Ioannis Koktzoglou, Ph.D.[1,2] and **Robert R. Edelman, M.D.**[1,3]

[1]Department of Radiology, NorthShore University HealthSystem, Evanston, IL

[2]The University of Chicago Pritzker School of Medicine, Chicago, IL

[3]Northwestern University Feinberg School of Medicine, Chicago, IL

Abstract

Purpose—To evaluate the combination of nonenhanced quiescent-interval slice-selective (QISS) magnetic resonance angiography (MRA) with super-resolution reconstruction for portraying the intracranial arteries.

Methods—The intracranial arteries of seven volunteers were imaged at 3 Tesla using QISS MRA acquired with a flow-compensated fast low-angle shot (FLASH) readout and thin overlapping slices. The impacts of super-resolution reconstruction and various acquisition parameters on the delineation of intracranial arteries were quantified using four metrics: arterial-to-background contrast-to-noise ratio (CNR), arterial-to-background contrast, arterial sharpness, and arterial full-width-at-half-maximum (FWHM). Three-dimensional time-of-flight (TOF) MRA was also acquired.

Results—For similar voxel sizes, QISS MRA displayed the intracranial arteries with an arterial-to-background contrast that exceeded 3D TOF MRA by 59–84%, depending on the k-space sampling trajectory ($P<0.001$). Super-resolution reconstruction improved CNR, contrast, and sharpness, while reducing arterial FWHM ($P<0.001$). Cardiac triggering provided minimal benefits, while Cartesian sampling provided higher CNR than radial sampling for multi-shot QISS ($P<0.05$). Scan time for a complete intracranial MRA was <90 seconds using an ungated single-shot QISS acquisition.

Conclusion—Thin, overlapping-slice QISS leveraging super-resolution reconstruction is a flexible approach for intracranial MRA that provides competitive image quality to standard-of-care 3D TOF, with the potential for reduced sensitivity to in-plane flow saturation and motion artifacts.

Keywords

Angiography; intracranial; super-resolution; MRA

To Whom Correspondence Should be Addressed: Ioannis Koktzoglou, Ph.D. NorthShore University HealthSystem, Walgreen Jr. Building, G507, 2650 Ridge Ave. Evanston, IL 60201, Tel: (847) 570-4288, Fax: (847) 570-2942, ikoktzoglou@gmail.com.

Author Manuscript Author Manuscript Author Manuscript Author Manuscript

INTRODUCTION

Magnetic resonance angiography (MRA) using 3D time-of-flight (TOF) is a mainstay of diagnosis for evaluating suspected pathology of the intracranial arteries. 3D TOF is a capable method that has seen little change in over two decades despite limitations relating to spin saturation and sensitivity to patient motion (1,2). Despite its widespread use in body applications and for evaluation of the extracranial carotid arteries, contrast-enhanced MRA is seldom applied for the intracranial circulation. Moreover, in patients with renal insufficiency, there are potential risks of administering gadolinium-based contrast media including nephrogenic systemic fibrosis (3) and gadolinium retention in the bones and brain (4–6).

There has been considerable progress in developing nonenhanced MRA techniques for extracranial applications (7–9). Within this context, quiescent-interval slice-selective (QISS), which was initially proposed for lower-extremity MRA because of its speed, ease of use, and ability to depict slow flow (10), has recently shown promise for portraying the extracranial carotid arteries (11). The QISS method, however, has not yet been applied to the brain where arteries are smaller in diameter and more tortuous.

In principle, QISS MRA might have potential benefits for evaluation of the intracranial arteries compared with 3D TOF. For instance, because thin slices are sequentially acquired, QISS MRA would be expected to show less severe artifacts from in-plane saturation effects than 3D TOF. Saturation effects are a particular concern in older patients, since flow velocities decrease with age (12). In addition, whereas brief periods of patient motion will degrade a small minority of QISS slices, all slices in the imaging volume will tend to be degraded using 3D TOF.

Nonetheless, portrayal of the intracranial arteries with QISS, a 2D technique, requires the acquisition of very thin slices, preferably <1 mm in thickness. Acquisition of such thin slices is often difficult because of system gradient limitations, undesirably long echo times and low signal-to-noise ratio. Thus, the use of non-traditional strategies for improving slice resolution in QISS MRA, such as super-resolution reconstruction of overlapping slices (13), could be beneficial. Super-resolution reconstruction leverages overlapping lower-resolution image data to improve spatial resolution. Although super-resolution reconstruction has shown promise in initial, albeit limited, MRI applications (14–16), the approach has not been applied to QISS MRA.

This study had three objectives. A principal objective was to examine the feasibility of intracranial 2D QISS MRA. A second objective was to determine whether super-resolution reconstruction in the slice direction could improve arterial delineation. A final objective of this study was to examine the impacts of various acquisition parameters on intracranial QISS MRA, including the applied k-space sampling trajectory, the presence or absence of physiologic triggering, the image acquisition speed, and the acquired in-plane spatial resolution.

Author Manuscript Author Manuscript Author Manuscript Author Manuscript

METHODS

Human Subjects and Imaging System

This study was approved by our institutional review board and all participants provided written informed consent. Magnetic resonance imaging of 7 volunteers (4 male, 3 female, age range = 24–53 years) was performed on a commercially available 3 Tesla system (MAGNETOM Skyra Fit, Siemens Healthcare, Erlangen) equipped with a 64-channel head and neck coil.

QISS Imaging Protocol

Intracranial QISS MRA was implemented similar to prior work aimed at portraying the extracranial carotid arteries (11), using a flow-compensated fast low-angle shot (FLASH) readout, slice-selective inversion-recovery based suppression of background tissue, and without chemically-selective fat suppression. In brief, the QISS MRA technique applies selective inversion RF pulses to suppress the appearance of in-slice and venous spins, and portrays arteries based on inflow into the imaging slice during either a quiescent interval (i.e. dedicated wait time) or during the data acquisition period. Each data acquisition period collects multiple phase-encoding lines (Cartesian sampling) or views (radial sampling). The time period spanning from the start of the first slice-selective inversion RF pulse to the end of the data acquisition period constitutes one QISS “shot.”

Overlapping slices were acquired in this study to yield QISS data suitable for super-resolution reconstruction. Baseline imaging parameters for intracranial QISS MRA were as follows: ungated image acquisition, TR/TE/flip=10 ms/4.6 ms/30°, acquired (zero-filled interpolated) in-plane voxel size of 1.0(0.5) mm×1.0(0.5) mm, 256 mm×256 mm field of view, 128 1.4-mm-thick axial slices with 50% (0.7 mm) overlap, 3 shots per slice, acquisition of 64 lines/views per shot, shot duration of 670 ms, slice-selective inversion thickness of 2.1 mm, receiver bandwidth of 501 Hz/pixel, 340 ms delay between the inversion-recovery background suppression RF pulse and center of the imaging readout, superior tracking saturation for venous signal suppression (15 mm gap, 75 mm thickness), scan time 4 min 17s. No time delay was inserted between the end of the data acquisition and the application of the next slice-selective inversion.

Impact of QISS Acquisition Parameters

Beyond the baseline QISS imaging protocol with parameters listed above, the impacts of k-space sampling trajectory, the number of shots, in-plane spatial resolution, and electrocardiographic triggering were examined. The impact of the k-space sampling trajectory was tested by acquiring QISS with Cartesian sampling, as well as with radial sampling using a view angle increment of ≈15° providing azimuthal equidistant k-space coverage (17). To test the ability to shorten the acquisition time, the number of QISS shots for collecting one slice was varied from 1 to 3 (yielding a total of 64–192 Cartesian lines/radial views, respectively). To match the echo train lengths of their radial counterparts (i.e. 64 views per shot), single-shot Cartesian and 2-shot Cartesian QISS protocols used generalized autocalibrating partially parallel imaging (18) factors of 4 and 2, with 20 and 62 reference lines, respectively. The impact of physiologic triggering on QISS MRA was

Author Manuscript Author Manuscript Author Manuscript Author Manuscript

examined by acquiring the 3-shot protocols with and without electrocardiographic gating. The repetition interval for cardiac-gated acquisitions was one heartbeat (i.e. 1 R-to-R interval). Also tested were higher spatial resolution, ungated 3-shot radial and Cartesian QISS protocols providing an acquired (zero-filled interpolated) in-plane voxel size of 0.7(0.35) mm×0.7(0.35) mm over a 202 mm×202 mm field of view. For each protocol, a single QISS slice was acquired twice at the level of the horizontal segment of the middle cerebral artery for the purpose of noise estimation using the dual acquisition subtraction method (19).

Super-Resolution Reconstruction

To evaluate the impact of super-resolution reconstruction, QISS image sets were reconstructed without and with super-resolution reconstruction. Super-resolution reconstruction was implemented offline in MATLAB software (version 8.4, Mathworks Inc., Natick, MA) using the iterative back-projection algorithm described by Irani and Peleg (20). The Irani-Peleg algorithm was chosen because it is computationally efficient and, according to the results of Plenge et al. (16), approaches the performance of more computationally demanding algorithms. A detailed description of the algorithm as applied for resolution improvement in MRI is provided elsewhere (14,15). In brief, the algorithm starts with the creation of an initial guess for the super-resolution reconstructed volume, and then iterates, adjusting the super-resolution reconstructed volume to ensure consistency with the acquired lower-resolution data. The algorithm then iteratively back-projects the differences between downsampled versions of the reconstructed volume and the acquired lower-resolution data and stops when the mean squared differences between the acquired and downsampled super-resolution reconstructed data are minimized.

In the present work, super-resolution reconstruction was applied in the slice direction. In generating the final reconstructed volume, the algorithm was executed separately for every row (i.e. anterior-posterior plane) of the acquired stack of QISS images. The initial guess for the super-resolution reconstruction equaled the spatial average of the offset overlapping lower-resolution source slices (14). The down-sampling and back-projection kernels used during super-resolution reconstruction equaled [0.25, 0.50, 0.25]; this kernel apportioned a 50% weight to the lower-resolution source slice centered at the reconstructed location, and 25% weights to the immediately adjacent lower-resolution source slices. To suppress noise amplification, voxels in the reconstructed slices with less than 2% signal change between iterations were not updated in subsequent iterations (20). Convergence was obtained in ≤5 iterations. Reconstruction time was approximately 60 s per volume on a 2.3 GHz central processing unit (i5-2410M, Intel Corporation, Santa Clara, CA).

Comparative Time-of-Flight Angiography

Three-dimensional TOF MRA was acquired in all subjects for comparative purposes. Two TOF protocols were collected, equaling the spatial resolutions and approximately matching the coverages and scan times of the QISS protocols. Imaging parameters for the lower-resolution protocol were: TR/TE/flip of 21.0 ms/3.4 ms/20°, flow compensation, asymmetric echo, 126 axial slices acquired in 5 slabs, acquired (zero-filled interpolated) voxel size of 1.0(0.5) mm×1.0(0.5) mm×1.4 mm(0.7 mm), 200 mm×256 mm field of view, generalized

Author Manuscript Author Manuscript Author Manuscript Author Manuscript

autocalibrating partially parallel imaging factor of 2 with 32 reference lines, scan time of 3min 56s, receiver bandwidth of 186 Hz/pixel, tilted optimized non-saturating excitation with 70% ramp, superior tracking saturation (10 mm gap, 40 mm thickness), 3D centric reordering. Parameters for the higher-resolution TOF protocol were identical except for the following: 136 axial slices acquired in 4 slabs, acquired (zero-filled interpolated) voxel size of 0.7(0.35) mm×0.7(0.35) mm ×1.4(0.7) mm, 200 mm×224 mm field of view, scan time of 4 min 54s, 7/8th partial Fourier in the slice direction. For the purpose of noise estimation, a single TOF slab was acquired twice at the level of the horizontal segment of the middle cerebral artery.

Image Analysis

Image analysis included computation of arterial-to-background contrast-to-noise ratio (CNR) in the horizontal (M1) segment of the right middle cerebral artery. In calculating CNR, image noise was estimated using the dual acquisition subtraction method (19). CNR was computed as $(S_A\text{-}S_B)/\sigma_B$, where S_A and S_B denote the mean signals in the arterial segment and in a region of background brain tissue, respectively, and σ_B is the noise of the background region. Additionally, arterial-to-background contrast for the horizontal (M1), and insular (M2), opercular (M3) and cortical (M4) segments of the right middle cerebral artery (MCA) were calculated as $S_A/S_B–1$.

To quantify the impact of super-resolution reconstruction on vessel localization and definition in the slice (i.e. head-foot) direction, arterial full-width-at-half-maximum (FWHM) and sharpness in the slice direction were computed by analysis of signal profiles through the aforementioned four segments of the MCA. Arterial sharpness was measured as in prior work (21), as the inverse of the distance separating the 20th and 80th percentile locations on both edges of the artery. Analyses were done in ImageJ software (version 1.51d, National Institutes of Health, Bethesda, MD).

Statistical Analysis

Unless noted otherwise, all statistical comparisons were done after matching for the use of cardiac triggering, the k-space sampling trajectory, the number of imaging shots, and the acquired in-plane spatial resolution. Differences in quantitative data were detected using either paired t-tests or Wilcoxon signed-rank tests, depending on data normality. Relationships between quantitative variables were assessed using iterative reweighted least-squares linear regression analysis, which provides robustness against outliers (22). Statistical analyses were done in R software (version 3.3.2, The R Foundation for Statistical Computing, Vienna). Two-tailed P values less than 0.05 were considered statistically significant.

RESULTS

Technical Feasibility and Impact of Super-Resolution Reconstruction

QISS MRA readily portrayed the intracranial arteries in all subjects. Figure 1 illustrates the impact of super-resolution reconstruction on intracranial QISS MRA. Compared with conventional reconstruction, super-resolution reconstruction improved arterial delineation in

Author Manuscript Author Manuscript Author Manuscript Author Manuscript

the slice direction, in both large and small intracranial arteries. Combining data across all image acquisition implementations (i.e. spatial resolutions, sampling trajectories, gating configurations, numbers of imaging shots) and intracranial arterial segments, super-resolution reconstruction provided a 13% mean increase in arterial-to-background CNR ($P<0.001$, n=70), a 17% mean increase in arterial-to-background contrast ($P<0.001$, n=280), a 21% mean increase in arterial sharpness ($P<0.001$, n=280), and a 7% mean decrease in arterial FWHM ($P<0.001$, n=280) (Figure 2). The statistical significance of these findings held true for both acquired in-plane spatial resolutions (1.0 mm and 0.7 mm), all three tested shot lengths, as well as for all segments of the middle cerebral arteries ($P<0.001$, all comparisons). A summary of quantitative metrics obtained with standard and super-resolution reconstruction stratified by arterial location and acquired in-plane spatial resolution are provided in Table 1.

Based on the beneficial impact of super-resolution reconstruction, results presented hereafter are derived solely from data obtained with super-resolution reconstruction.

Impact of Number of Shots and K-Space Sampling Trajectory

Figure 3 shows the appearance of ungated super-resolution intracranial QISS MRA and its dependence on the number of acquired shots and k-space sampling trajectory. Intracranial arteries were displayed at all shot lengths tested, but 2- and 3-shot configurations provided the best display of both large and small arterial segments. Ungated single-shot QISS using a Cartesian k-space sampling trajectory demonstrated arterial pulsation artifact in the distal internal carotid and basilar arteries, which was less pronounced with the use of radial sampling.

The following results were obtained after matching for all varied parameters such as the acquired in-plane spatial resolution, k-space trajectory, number of imaging shots, and the use of cardiac triggering. Arterial sharpness and arterial FWHM did not differ across the three shot lengths tested (P=NS, n=56). Arterial-to-background CNR increased with the number of shots, with single-shot and 2-shot QISS MRA providing 46% and 78% percent of the CNR of 3-shot QISS ($P<0.001$, n=14, both comparisons). Arterial-to-background contrast demonstrated a more mild dependence on the number of imaging shots, with single-shot and 2-shot imaging providing 89% ($P<0.001$, n=56) and 95% ($P<0.05$, n=56) of the arterial contrast of 3-shot QISS MRA.

The impact of k-space trajectory on quantitative indices is summarized in Figure 4. Across the three shot lengths tested, radial sampling provided, on average, 14% lower arterial-to-background CNR ($P<0.001$, n=35) and 22% higher arterial-to-background contrast ($P<0.001$, n=140) than Cartesian sampling. Further examination of the data revealed that 2-shot and 3-shot Cartesian imaging provided 32% and 24% increased CNR than radial sampling ($P<0.05$, n=14, both comparisons), whereas single-shot radial imaging matched the CNR of single-shot Cartesian sampling (P=NS, n=7). Radial sampling provided a small 1.6% decrease in arterial FWHM with respect to Cartesian sampling ($P<0.05$; n=140). No difference in arterial sharpness between radial and Cartesian sampling was found (P=NS; n=140).

Author Manuscript Author Manuscript Author Manuscript Author Manuscript

Impact of Physiologic Triggering

Figure 5 shows the impact of physiologic triggering on super-resolution intracranial QISS MRA. Ungated and cardiac-gated super-resolution 3-shot QISS MRA provided image appearances that were similar to each other, and competitive with resolution-matched 3D TOF MRA. The mean acquisition time for cardiac-gated 3-shot QISS MRA was 5 min 28 s, 28% longer on average than ungated QISS imaging. No significant differences in arterial-to-background CNR and arterial sharpness between cardiac-gated and ungated QISS were found in any MCA segment. However, small gains in arterial-to-background contrast were found with cardiac gating in the M1 (9.3 versus 8.57, $P<0.05$, n=14), M2 (6.68 versus 5.74, $P<0.01$, n=14) and M3 (4.17 versus 3.48, $P<0.01$, n=14) segments of the middle cerebral arteries. Arterial FWHM was also measured slightly larger in the M3 segment with cardiac gating (1.94 mm versus 1.89 mm, $P<0.05$, n=14) than without.

Higher Resolution Imaging and Comparisons with 3D TOF

Figure 6 shows the feasibility of intracranial QISS MRA with sub-millimeter in-plane resolution. Compared to QISS MRA acquired with 1.0 mm in-plane spatial resolution, 0.7 mm resolution imaging improved small vessel detail, albeit with a 48% drop in CNR ($P<0.001$, n=14), a 1% drop in arterial contrast ($P<0.05$, n=56), and 3% drop in arterial FWHM ($P<0.05$, n=56).

With respect to resolution-matched 3D TOF, ungated 3-shot QISS MRA using radial and Cartesian trajectories provided, on average, 39% and 24% lower arterial-to-background CNR ($P<0.01$, n=14, both comparisons), respectively. Mean values of arterial sharpness trended 9% larger when using radial ($P=0.052$, n=56) and Cartesian ($P<0.05$, n=56) sampling, whereas arterial FWHM measures with radial/Cartesian sampling were 10%/7% smaller than those provided by 3D TOF ($P<0.001$, n=56, both comparisons). Most strikingly, arterial-to-background contrast values provided by QISS using radial and Cartesian k-space sampling were 84% and 59% larger than those of 3D TOF, respectively ($P<0.001$, n=56, both comparisons).

DISCUSSION

In this study, we applied nonenhanced QISS MRA in combination with super-resolution reconstruction to portray the intracranial circulation. Intracranial QISS MRA was found to be feasible and, with respect to conventional image reconstruction, super-resolution reconstruction significantly improved arterial definition in the slice direction and arterial-to-background CNR. We also observed that QISS MRA provided near-complete suppression of background signal, and therefore, stark arterial-to-background contrast without the need for signal subtraction. When spatial resolution was made near isotropic, QISS MRA allowed the creation of multi-planar reconstructions without obvious loss of quality.

QISS MRA has previously been applied to evaluate the lower extremity (10), carotid (11) and coronary arteries (23). To our knowledge, this is the first application of QISS MRA for portraying the intracranial arteries. A difficulty in applying QISS MRA, a 2D method, to visualize the small and tortuous intracranial arteries has been spatial resolution in the slice-

Author Manuscript Author Manuscript Author Manuscript Author Manuscript

select direction. Herein, we showed that super-resolution reconstruction of overlapping slices with sub-millimeter spacing addresses this problem and improves arterial definition with respect to standard (i.e. non-super-resolution) reconstruction. It should be noted that super-resolution reconstruction as applied in the present study requires the acquisition of overlapping slice data, and therefore could not be applied to improve the slice resolution of 3D TOF MRA.

Outside the brain, QISS MRA is traditionally acquired with the use of cardiac triggering to ensure that imaging occurs in diastole, as well as a balanced steady-state free precession readout (24). However, the use of cardiac triggering is inconvenient for intracranial MRA as it entails extra time for lead placement and therefore reduces exam efficiency. We found that cardiac triggering was not needed for QISS MRA of the intracranial arteries, which differs from our experience within the peripheral arteries. The use of a balanced steady-state free precession imaging is problematic for imaging the intracranial circulation due to its sensitivity to off-resonance artifacts, which are especially troublesome near the skull base and the paranasal sinuses. In addition, there are artifacts due to steady-state signal contributions from spins that have flowed through and out of the slice (25). To address these issues, a flow-compensated FLASH readout was used instead of a balanced steady-state free precession readout.

A notable finding of our study was the near elimination of non-vascular background signal with QISS MRA, without the need for subtraction-based processing (26). We attribute the robust suppression of background signal to the combination of an in-plane inversion RF pulse, the selection of an inversion time (340 ms) that almost nulls the appearance of non-vascular background tissue, and the use of a FLASH readout which saturates stationary tissues with long T_1. Depending on the k-space sampling trajectory, arterial-to-background contrast of QISS FLASH MRA was ≈1.6–1.8-fold greater than that of 3D TOF. The stark angiographic contrast provided by QISS MRA enabled the use of thick maximum intensity projection images for visualizing intracranial arteries, with little loss of small vessel conspicuity.

Both radial and Cartesian k-space trajectories were found capable of portraying the intracranial arteries with QISS MRA. With respect to radial sampling, Cartesian sampling provided larger CNR for 2-shot and 3-shot QISS imaging, but not for single-shot imaging. The observed CNR advantage of multi-shot Cartesian QISS is in general consistent with the theoretical signal-to-noise advantage of Cartesian versus radial sampling (27). So long as patient motion is not a major concern, Cartesian sampling appears advantageous for multi-shot intracranial QISS MRA, solely on the basis of CNR considerations.

Radial sampling, however, confers less sensitivity to motion and flow artifact than Cartesian sampling due to oversampling of central k-space (27). Also, as the spatial resolution with radial sampling is dominated by the readout resolution (rather than the number of acquired phase encoding lines, as is the case with Cartesian sampling) (28), radial sampling avoids the need to apply parallel imaging reconstruction techniques during highly-undersampled scenarios, as was the case with single-shot and 2-shot radial QISS MRA in this study. Moreover, parallel imaging reconstruction, which is needed to recover spatial resolution with

Author Manuscript Author Manuscript Author Manuscript Author Manuscript

Cartesian sampling, is associated with noise amplification that tends to increase supra-linearly with the degree of undersampling (29). These strengths of radial sampling were reflected in the reduced pulsation artifact and comparable CNR measured during ungated single-shot QISS MRA.

A limitation of this study was that it was restricted to the imaging of healthy subjects. Future work should seek to evaluate and validate the super-resolution QISS protocol in patients with known or suspected cerebrovascular disease. Study of a larger group of human subjects would also help elucidate whether QISS ameliorates the age-dependent saturation of small vessels previously reported with 3D TOF (12), as well as identify the impacts of other potential covariates such as gender. Anecdotally, we did observe substantially improved small intracranial arterial definition with QISS MRA in the oldest subject who participated in the study (Figure 5). With respect to 3D TOF, a weakness of 2D QISS was lower CNR in the horizontal M1 segment of the middle cerebral artery. This lower CNR, probably attributable to QISS being a 2D (as opposed to a 3D) imaging technique, could be problematic when attempting to image the intracranial arteries at very high spatial resolution (e.g, ≤0.5 mm in-plane). Finally, due to the lack of gold standard digital subtraction angiography, it is not possible to determine whether QISS or TOF provided more accurate assessments of arterial caliber in this study.

We anticipate that the super-resolution reconstruction technique used in this study could be beneficial for QISS MRA when applied to other vascular territories. In addition, the use of greater slice overlap (e.g., 66% or 75%, instead of 50% as used here), and more sophisticated super-resolution reconstruction algorithms may allow for further improvements in reconstructed slice resolution. With regard to the latter point, however, we did not observe improved image quality with the use of a more computationally demanding maximum a-posteriori super-resolution reconstruction algorithm (30,31). Also, rather than applying super-resolution reconstruction serially on a planar (i.e. 2D) basis, as was done in the present study, reconstruction over the entire volume in each iteration may improve computational efficiency and reconstruction uniformity. Lastly, improvements in image quality and acquisition speed of intracranial QISS MRA may be possible with use of non-Cartesian parallel imaging reconstruction (32), compressed sensing reconstruction (33) and simultaneous multi-slice imaging techniques (34).

CONCLUSION

In conclusion, we found that the combination of thin-slice QISS MRA with super-resolution reconstruction provides competitive image quality to standard-of-care 3D TOF, with the potential for reduced sensitivity to in-plane flow saturation and motion artifacts. The use of super-resolution reconstruction was beneficial for improving arterial-to-background contrast and contrast-to-noise ratio, as well as arterial definition in the slice direction. Future studies should seek to corroborate these results in patients with cerebrovascular disease.

Acknowledgments

The authors thank Drs. Shivraman Giri and Jianing Pang of Siemens Healthineers for technical support. This work was supported in part by National Institutes of Health grant R01 HL130093.

Author Manuscript Author Manuscript Author Manuscript Author Manuscript

References

1. Davis WL, Warnock SH, Harnsberger HR, Parker DL, Chen CX. Intracranial MRA: single volume vs. multiple thin slab 3D time-of-flight acquisition. J Comput Assist Tomogr. 1993; 17(1):15–21. [PubMed: 8419427]
2. Davis WL, Blatter DD, Harnsberger HR, Parker DL. Intracranial MR angiography: comparison of single-volume three-dimensional time-of-flight and multiple overlapping thin slab acquisition techniques. AJR Am J Roentgenol. 1994; 163(4):915–920. [PubMed: 8092035]
3. Kuo PH, Kanal E, Abu-Alfa AK, Cowper SE. Gadolinium-based MR contrast agents and nephrogenic systemic fibrosis. Radiology. 2007; 242(3):647–649. [PubMed: 17213364]
4. McDonald RJ, McDonald JS, Kallmes DF, Jentoft ME, Murray DL, Thielen KR, Williamson EE, Eckel LJ. Intracranial gadolinium deposition after contrast-enhanced MR imaging. Radiology. 2015; 275(3):772–782. [PubMed: 25742194]
5. Kanda T, Fukusato T, Matsuda M, Toyoda K, Oba H, Kotoku J, Haruyama T, Kitajima K, Furui S. Gadolinium-based contrast agent accumulates in the brain even in subjects without severe renal dysfunction: evaluation of autopsy brain specimens with inductively coupled plasma mass spectroscopy. Radiology. 2015; 276(1):228–232. [PubMed: 25942417]
6. Murata N, Gonzalez-Cuyar LF, Murata K, Fligner C, Dills R, Hippe D, Maravilla KR. Macrocyclic and other non-group 1 gadolinium contrast agents deposit low levels of gadolinium in brain and bone tissue: preliminary results from 9 patients with normal renal function. Invest Radiol. 2016; 51(7):447–453. [PubMed: 26863577]
7. Miyazaki M, Lee VS. Nonenhanced MR angiography. Radiology. 2008; 248(1):20–43. [PubMed: 18566168]
8. Wheaton AJ, Miyazaki M. Non-contrast enhanced MR angiography: physical principles. J Magn Reson Imaging. 2012; 36(2):286–304. [PubMed: 22807222]
9. Lim RP, Koktzoglou I. Noncontrast magnetic resonance angiography: concepts and clinical applications. Radiol Clin North Am. 2015; 53(3):457–476. [PubMed: 25953284]
10. Hodnett PA, Koktzoglou I, Davarpanah AH, Scanlon TG, Collins JD, Sheehan JJ, Dunkle EE, Gupta N, Carr JC, Edelman RR. Evaluation of peripheral arterial disease with nonenhanced quiescent-interval single-shot MR angiography. Radiology. 2011; 260(1):282–293. [PubMed: 21502384]
11. Koktzoglou I, Murphy IG, Giri S, Edelman RR. Quiescent interval low angle shot magnetic resonance angiography of the extracranial carotid arteries. Magn Reson Med. 2016; 75(5):2072–2077. [PubMed: 26072706]
12. Kusunoki K, Oka Y, Saito M, Sadamoto K, Sakaki S, Miki H, Nagasawa K. Changes in visibility of intracranial arteries on MRA with normal ageing. Neuroradiology. 1999; 41(11):813–819. [PubMed: 10602853]
13. Park SC, Park MK, Kang MG. Super-resolution image reconstruction: a technical overview. IEEE Signal Processing Magazine. 2003; 20(3):21–36.
14. Peled S, Yeshurun Y. Superresolution in MRI: application to human white matter fiber tract visualization by diffusion tensor imaging. Magn Reson Med. 2001; 45(1):29–35. [PubMed: 11146482]
15. Greenspan H, Oz G, Kiryati N, Peled S. MRI inter-slice reconstruction using super-resolution. Magn Reson Imaging. 2002; 20(5):437–446. [PubMed: 12206870]
16. Plenge E, Poot DH, Bernsen M, Kotek G, Houston G, Wielopolski P, van der Weerd L, Niessen WJ, Meijering E. Super-resolution methods in MRI: can they improve the trade-off between resolution, signal-to-noise ratio, and acquisition time? Magn Reson Med. 2012; 68(6):1983–1993. [PubMed: 22298247]
17. Edelman RR, Giri S, Murphy IG, Flanagan O, Speier P, Koktzoglou I. Ungated radial quiescent-inflow single-shot (UnQISS) magnetic resonance angiography using optimized azimuthal equidistant projections. Magn Reson Med. 2014; 72(6):1522–1529. [PubMed: 25257379]
18. Griswold MA, Jakob PM, Heidemann RM, Nittka M, Jellus V, Wang J, Kiefer B, Haase A. Generalized autocalibrating partially parallel acquisitions (GRAPPA). Magn Reson Med. 2002; 47(6):1202–1210. [PubMed: 12111967]

Author Manuscript Author Manuscript Author Manuscript Author Manuscript

19. Firbank MJ, Coulthard A, Harrison RM, Williams ED. A comparison of two methods for measuring the signal to noise ratio on MR images. Phys Med Biol. 1999; 44(12):N261–264. [PubMed: 10616158]
20. Irani M, Peleg S. Improving resolution by image registration. CVGIP: Graphical Models and Image Processing. 1991; 53(3):231–239.
21. Li D, Carr JC, Shea SM, Zheng J, Deshpande VS, Wielopolski PA, Finn JP. Coronary arteries: magnetization-prepared contrast-enhanced three-dimensional volume-targeted breath-hold MR angiography. Radiology. 2001; 219(1):270–277. [PubMed: 11274569]
22. Venables WN, Ripley BD. Modern Applied Statistics with S. York. 2002
23. Edelman RR, Giri S, Pursnani A, Botelho MP, Li W, Koktzoglou I. Breath-hold imaging of the coronary arteries using quiescent-interval slice-selective (QISS) magnetic resonance angiography: pilot study at 1.5 Tesla and 3 Tesla. J Cardiovasc Magn Reson. 2015; 17:101. [PubMed: 26597281]
24. Edelman RR, Sheehan JJ, Dunkle E, Schindler N, Carr J, Koktzoglou I. Quiescent-interval single-shot unenhanced magnetic resonance angiography of peripheral vascular disease: technical considerations and clinical feasibility. Magn Reson Med. 2010; 63(4):951–958. [PubMed: 20373396]
25. Markl M, Alley MT, Elkins CJ, Pelc NJ. Flow effects in balanced steady state free precession imaging. Magn Reson Med. 2003; 50(5):892–903. [PubMed: 14586999]
26. Nishimura DG, Macovski A, Pauly JM, Conolly SM. MR angiography by selective inversion recovery. Magn Reson Med. 1987; 4(2):193–202. [PubMed: 3561250]
27. Glover GH, Pauly JM. Projection reconstruction techniques for reduction of motion effects in MRI. Magn Reson Med. 1992; 28(2):275–289. [PubMed: 1461126]
28. Peters DC, Korosec FR, Grist TM, Block WF, Holden JE, Vigen KK, Mistretta CA. Undersampled projection reconstruction applied to MR angiography. Magn Reson Med. 2000; 43(1):91–101. [PubMed: 10642735]
29. Pruessmann KP, Weiger M, Scheidegger MB, Boesiger P. SENSE: sensitivity encoding for fast MRI. Magn Reson Med. 1999; 42(5):952–962. [PubMed: 10542355]
30. Elad M, Feuer A. Restoration of a single superresolution image from several blurred, noisy, and undersampled measured images. IEEE Transactions on Image Processing. 1997; 6(12):1646–1658. [PubMed: 18285235]
31. Multi-Frame Super-Resolution Toolbox. Department of Computer Science, Friedrich-Alexander-Universität Erlangen-Nürnberg; Version 1.6.1https://www5.cs.fau.de/research/software/multi-frame-super-resolution-toolbox/. Published September 2016. Accessed October 2016
32. Pruessmann KP, Weiger M, Bornert P, Boesiger P. Advances in sensitivity encoding with arbitrary k-space trajectories. Magn Reson Med. 2001; 46(4):638–651. [PubMed: 11590639]
33. Lustig M, Donoho D, Pauly JM. Sparse MRI: The application of compressed sensing for rapid MR imaging. Magn Reson Med. 2007; 58(6):1182–1195. [PubMed: 17969013]
34. Setsompop K, Gagoski BA, Polimeni JR, Witzel T, Wedeen VJ, Wald LL. Blipped-controlled aliasing in parallel imaging for simultaneous multislice echo planar imaging with reduced g-factor penalty. Magn Reson Med. 2012; 67(5):1210–1224. [PubMed: 21858868]

Author Manuscript Author Manuscript Author Manuscript Author Manuscript

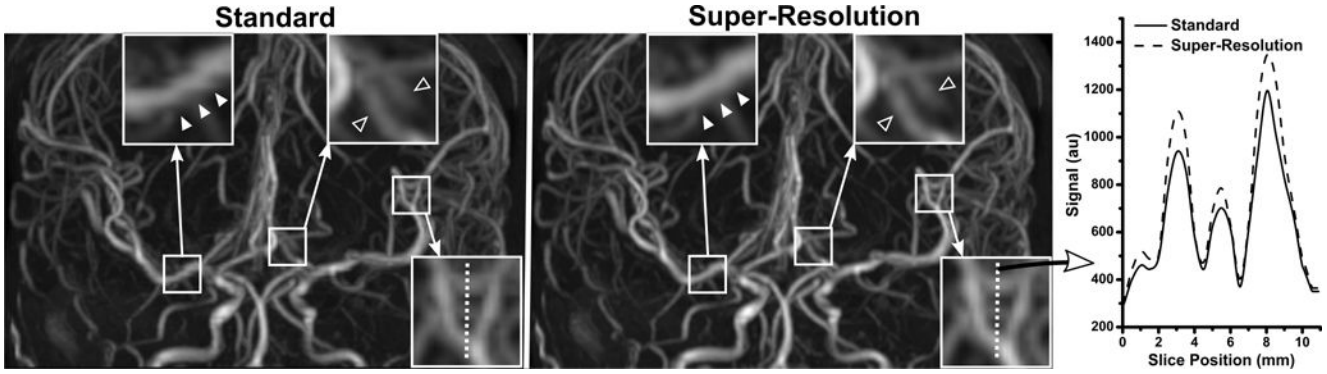

Figure 1.

Comparison of ungated 3-shot radial QISS MRA obtained with standard and super-resolution reconstruction in a 34-year-old female. Images are coronal maximum intensity projections; the slice direction is vertical. Three magnified regions illustrate the usefulness of super-resolution reconstruction throughout the field of view. Super-resolution reconstruction eliminates stair-step artifact seen in the right proximal middle cerebral artery with standard reconstruction (solid arrowheads), and improves the delineation of posterior cerebral arteries (hollow arrowheads). Signal profile analysis of a third magnified region in the slice direction (vertical dashed line) illustrates the improved arterial definition obtained with super-resolution reconstruction.

Author Manuscript Author Manuscript Author Manuscript Author Manuscript

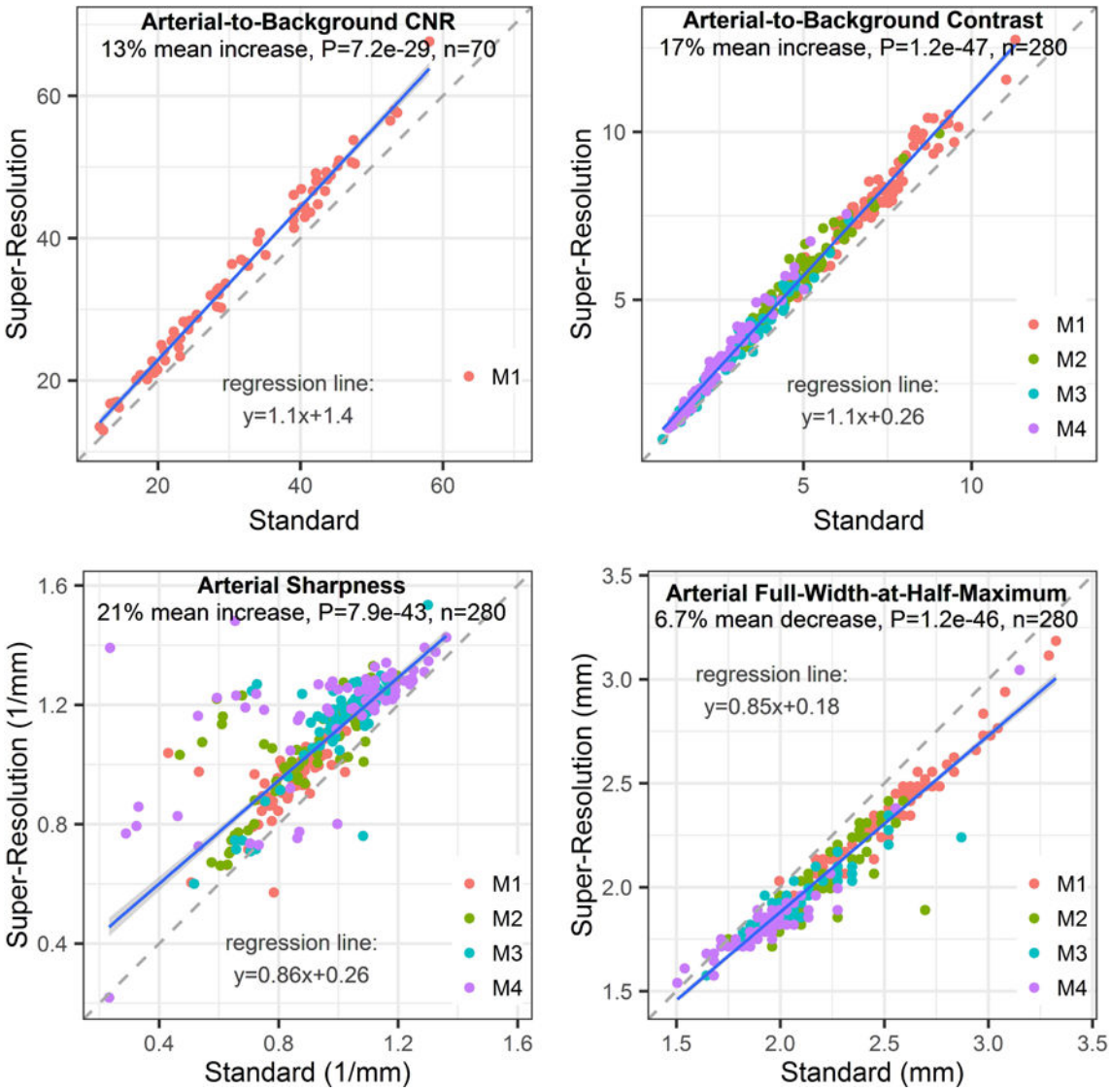

Figure 2.

Impact of standard versus super-resolution reconstruction on quantitative arterial metrics for QISS MRA. Super-resolution reconstruction resulted in statistically significant increases in arterial-to-background contrast-to-noise ratio (CNR), arterial-to-background contrast and arterial sharpness, and a significant reduction in arterial full-width-at-half-maximum. Plots show data from all QISS implementations irrespective of the k-space trajectory, acquired spatial resolution, number of imaging shots, and use of physiologic triggering. Legends refer to segments of the middle cerebral artery. Blue and dashed lines are the lines of robust regression and unity, respectively.

Author Manuscript Author Manuscript Author Manuscript Author Manuscript

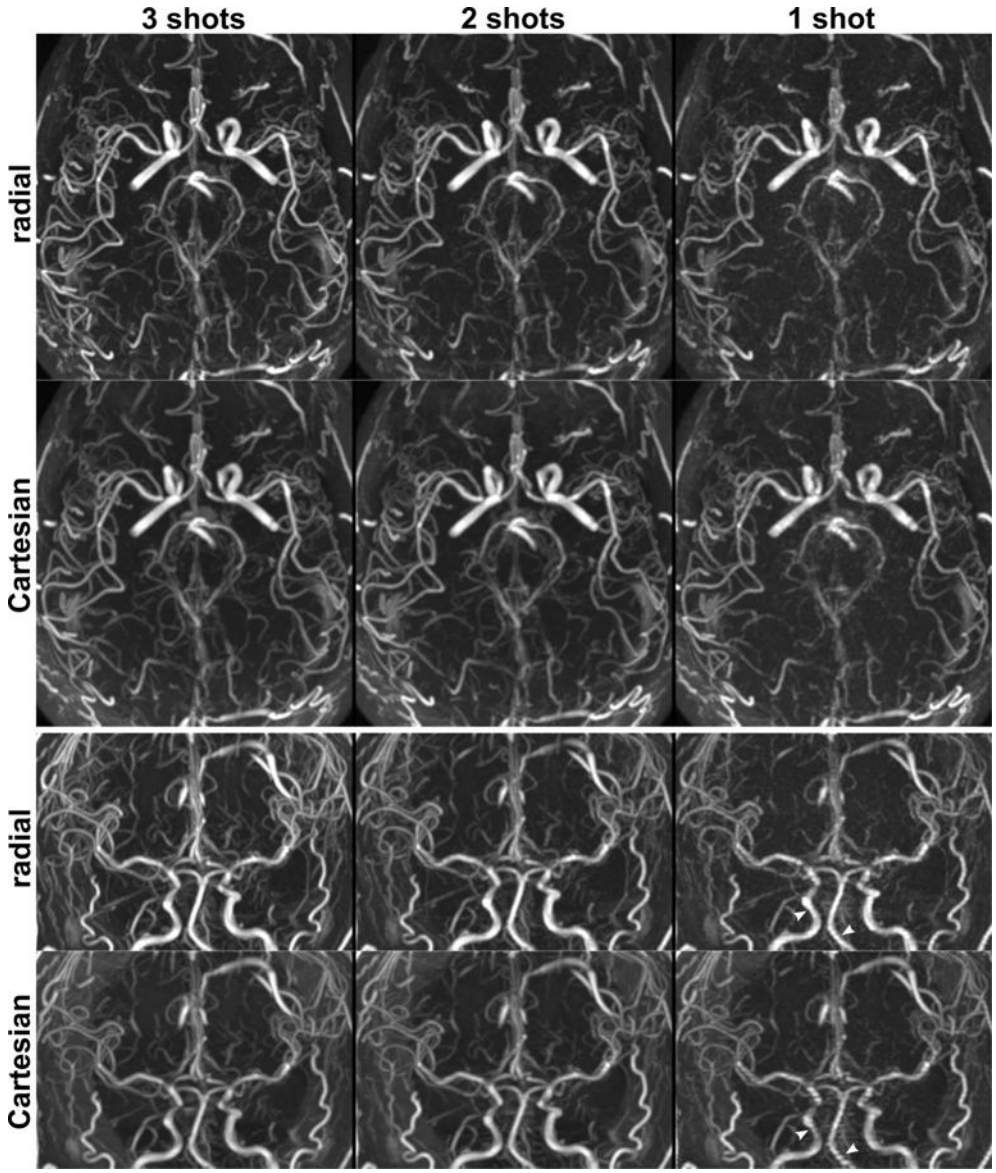

Figure 3.

Impacts of the number of imaging shots and the k-space sampling trajectory on ungated super-resolution intracranial QISS MRA in a 24-year-old male. Top and bottom panels show axial and coronal maximum intensity projections. Intracranial arteries are well seen with both k-space sampling trajectories with 3-shot and 2-shot imaging (scan times of 4 min 17 s and 2 min 52 s, respectively), whereas single-shot QISS (1 min 26 s) provides lower signal-to-noise and shows arterial pulsation artifact in the internal carotid and basilar arteries, which is ameliorated with the use of radial sampling (arrowheads in coronal views).

Author Manuscript Author Manuscript Author Manuscript Author Manuscript

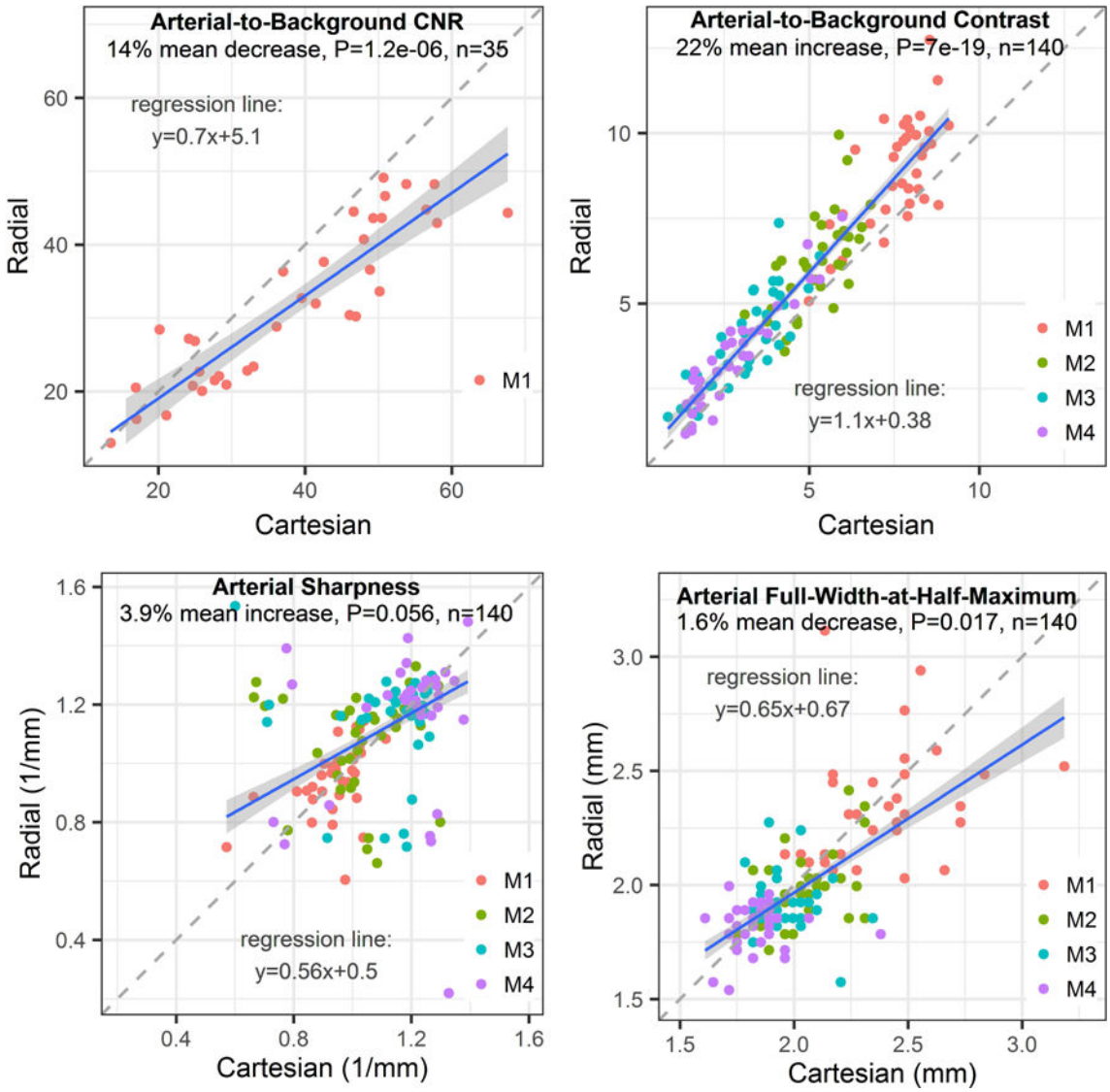

Figure 4.

Impact of the k-space sampling trajectory on quantitative metrics for data obtained with super-resolution reconstruction. Compared with Cartesian sampling, radial k-space sampling resulted in significant 10% median decreases 19% increases in arterial-to-background contrast-to-noise ratio (CNR) and contrast, respectively. No significant differences in arterial sharpness and full-width-at-half-maximum were found between trajectories. Plots display data from image sets obtained with super-resolution reconstruction, irrespective of the number of imaging shots, acquired spatial resolution, and use of physiologic triggering. Legends refer to segments of the middle cerebral artery. Blue and dashed lines are the lines of robust regression and unity, respectively.

Author Manuscript Author Manuscript Author Manuscript Author Manuscript

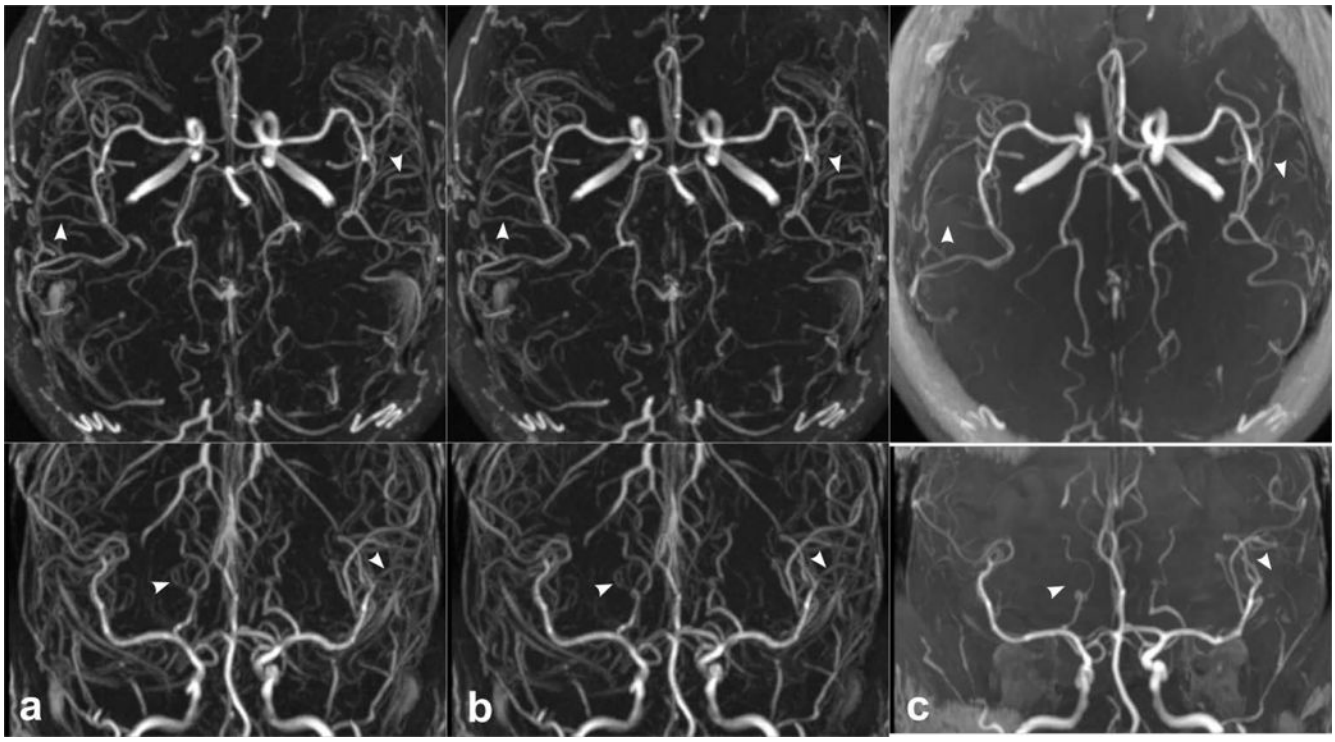

Figure 5.

Impact of cardiac triggering on image appearance for super-resolution QISS MRA in a 52-year-old female, in comparison with 3D TOF MRA. Images are axial (top panel) and coronal (bottom panel) maximum intensity projections. Three-shot radial QISS MRA acquired **(a)** with cardiac triggering (scan time 5 min 36 s) and **(b)** without cardiac triggering (scan time 4 min 17 s); there is minimal benefit from the use of cardiac triggering. **(c)** Resolution- and coverage-matched 3D TOF MRA (scan time 3 min 56 s). Compared with TOF, QISS demonstrates improved arterial-to-background contrast and display of small arterial detail (arrowheads).

Author Manuscript Author Manuscript Author Manuscript Author Manuscript

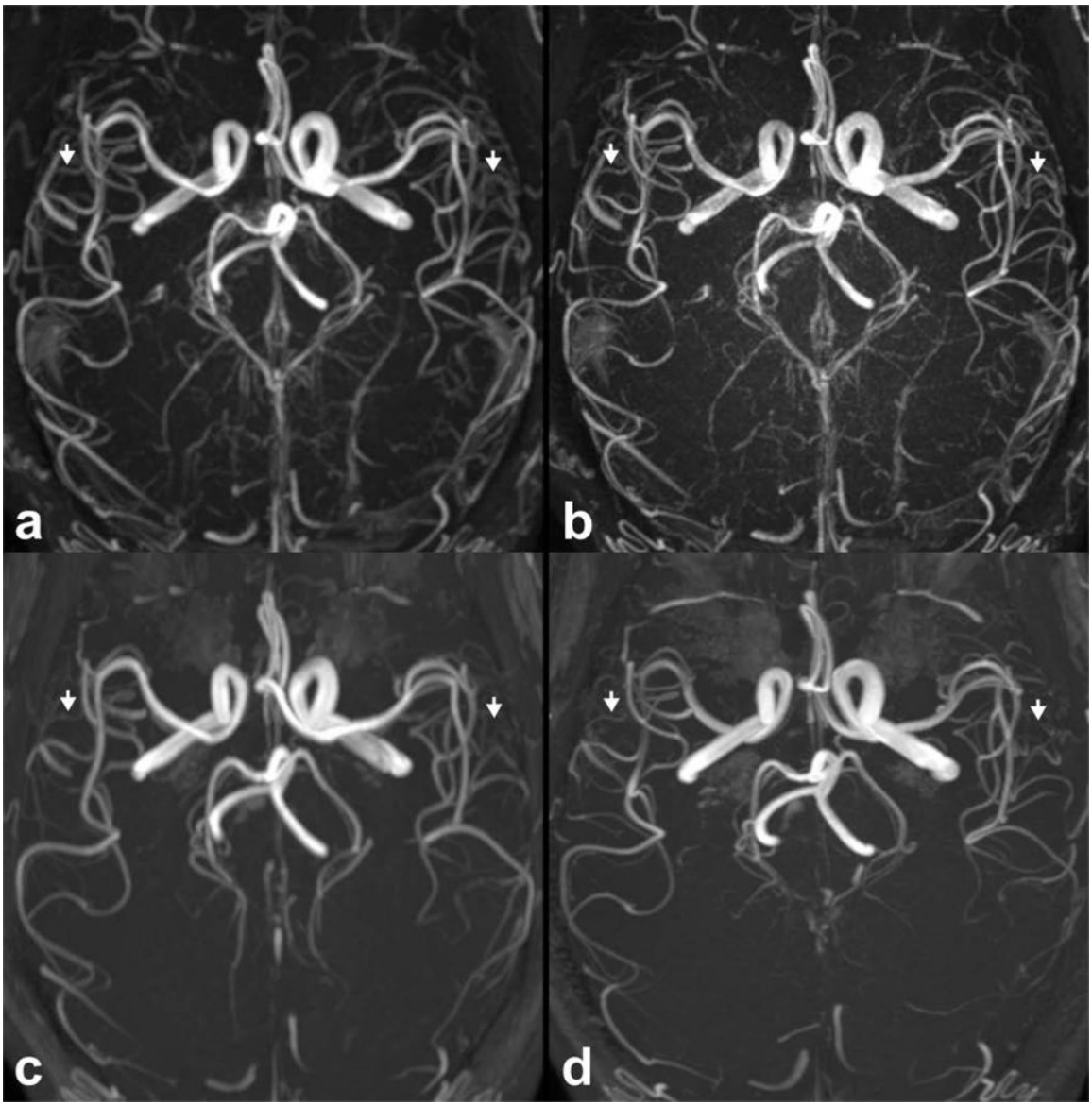

Figure 6.

Feasibility of intracranial super-resolution QISS MRA acquired with **(a)** 1.0 mm and **(b)** 0.7 mm in-plane spatial resolution in a 36-year-old male. Resolution-matched 3D TOF protocols are shown in **(c)** and **(d)**, respectively. Images are axial maximum intensity projections. Note the improved delineation of small intracranial arteries with QISS as compared to TOF MRA (arrows), at both spatial resolutions.

Author Manuscript Author Manuscript Author Manuscript Author Manuscript

Table 1

Summary of Quantitative QISS Parameters by Reconstruction Method, In-Plane Spatial Resolution, and Arterial Location

Metric	SR (mm)	n	MCA Segment	Standard Reconstruction	Super-Resolution Reconstruction	P-value
CNR	1.0	56	M1	34.0±11.7	38.0±12.8	<0.001
CNR	0.7	14	M1	21.0±3.93	23.9±4.27	<0.001
Contrast	1.0	56	M1	7.54±1.45	8.43±1.56	<0.001
Contrast	1.0	56	M2	4.99±1.23	5.82±1.33	<0.001
Contrast	1.0	56	M3	3.03±1.23	3.45±1.37	<0.001
Contrast	1.0	56	M4	2.48±1.16	3.04±1.45	<0.001
Contrast	0.7	14	M1	6.67±0.77	7.52±0.74	<0.001
Contrast	0.7	14	M2	4.72±0.74	5.41±0.79	<0.001
Contrast	0.7	14	M3	3.09±1.07	3.72±1.27	<0.001
Contrast	0.7	14	M4	2.61±1.08	3.20±1.33	<0.001
Sharpness	1.0	56	M1	0.84±0.13	0.94±0.12	<0.001
Sharpness	1.0	56	M2	0.87±0.18	1.02±0.16	<0.001
Sharpness	1.0	56	M3	1.00±0.16	1.14±0.17	<0.001
Sharpness	1.0	56	M4	0.99±0.29	1.15±0.23	<0.001
Sharpness	0.7	14	M1	0.85±0.11	0.98±0.12	<0.001
Sharpness	0.7	14	M2	0.98±0.18	1.12±0.20	<0.001
Sharpness	0.7	14	M3	0.98±0.13	1.12±0.17	<0.001
Sharpness	0.7	14	M4	0.89±0.26	1.22±0.16	<0.001
FWHM	1.0	56	M1	2.54±0.29	2.37±0.26	<0.001
FWHM	1.0	56	M2	2.23±0.20	2.05±0.17	<0.001
FWHM	1.0	56	M3	2.07±0.22	1.93±0.15	<0.001
FWHM	1.0	56	M4	1.96±0.23	1.85±0.19	<0.001
FWHM	0.7	14	M1	2.46±0.30	2.27±0.29	<0.001
FWHM	0.7	14	M2	2.08±0.20	1.92±0.17	<0.001
FWHM	0.7	14	M3	2.06±0.11	1.92±0.08	<0.001
FWHM	0.7	14	M4	1.96±0.22	1.82±0.19	<0.001

Magn Reson Med. Author manuscript; available in PMC 2019 February 01.

Author Manuscript Author Manuscript Author Manuscript Author Manuscript

Data presented as mean±standard deviation. SR=in-plane spatial resolution. MCA=middle cerebral artery. CNR=contrast-to-noise ratio. FWHM=full width at half maximum. Units for sharpness and FWHM are mm^{-1} and mm, respectively. Rows with 1.0 mm spatial resolution combine data regardless of the k-space sampling trajectory, number of imaging shots, and use of cardiac gating. Rows with 0.7 mm spatial resolution combine data obtained with both k-space sampling trajectories.